Behavior in oxidation at elevated temperature of 25Cr, 0.4C-6Ta-containing Ni and Co-based cast alloys versus their proportion in nickel and cobalt

Patrice Berthod, Zohra Himeur

Behavior in oxidation at elevated temperature of {25Cr, 0.4C-6Ta}-containing Ni and Co-based cast alloys versus their proportion in nickel and cobalt

Patrice Berthod and Zohra Himeur
Institut Jean Lamour (UMR CNRS 7198), department Chemistry and Physic of Solids and Surfaces
Faculty of Science and Technologies, B.P. 70239, 54506 Vandoeuvre-lès-Nancy, France
E-mail: pberthodcentralelille1987@orange.fr
Tel. (+33) 3 83 68 46 66
Fax (+33) 3 83 68 46 11

Postprint version of the article **Materials and Corrosion** 2018, 69, No. 6 pp. 703-713
DOI: 10.1002/maco.201709820

Summary:
A series of six alloys from Ni-25Cr-0.4C-6Ta to Co-25Cr-0.4C-6Ta with a progressive addition of Co in substitution to Ni were elaborated. They were tested for 24 hours at 1237°C in laboratory air. The corrosion products formed around the samples and the deterioration of the subsurface were analyzed to characterize the high temperature oxidation behavior of these alloys. Three of the studied alloys, the nickel-richest ones, well behaved until 24 hours at this temperature. Their external oxide scales were essentially composed of chromia. In contrast, locally, the three cobalt-richest alloys were starting to oxidize catastrophically. The significant worsening of the oxidation behavior from the 27wt.%Co-containing alloy to the 41wt.%Co-containing one suggests that a critical Co content exists between these two values.

Keywords:
Nickel-cobalt-chromium alloys; Tantalum carbides; Chromium carbides; High temperature Oxidation; Post-mortem characterization

1 Introduction

Metallic carbides, which are well known as being very hard particles [1,2], are frequently encountered in the microstructures of various metallic alloys elaborated and shaped by foundry. This is notably the case of some cast superalloys [3]. Carbides appearing during solidification feature among the first metallurgical ways of strengthening for cast metallic alloys designed for use at high temperature under mechanical stresses [4,5]. Chromium carbides were among the earliest carbides involved for enhancing high temperature strength. Later, tantalum carbides were also exploited to take part to the creep resistance, in the MarM-509 alloy [6-8] for instance. Different MC carbides may precipitate in cobalt-based [9] or nickel-based [10] polycrystalline alloys elaborated by induction melting. Among them, TaC carbides still remain interesting enough in many superalloys [11]. Indeed, at elevated temperatures, they remain intrinsically strong and particularly stable in term of volume fraction and morphology. This allows them to be particularly efficient for the strengthening of both grain boundaries and dendrites boundaries. In the cast superalloys containing chromium in high concentration for combatting both hot oxidation and hot corrosion [12,13] tantalum may be in competition with Cr in the formation of the strengthening carbides. In some case the stronger carbide-forming behavior of tantalum allows him to lead to an interdendritic network made of TaC carbides exclusively if the atomic contents in Ta and in C are equal. This is the case Co-based [14] and Fe-based [15] Cr-rich alloys. In contrast chromium carbides form together with TaC in Cr-rich nickel-based alloys containing Ta, even in the case of similar atomic contents in Ta and C [16]. It can be thought that replacing a part of nickel by cobalt in alloys based on nickel and containing chromium for high temperature chemical resistance purpose, may help TaC for predominating on chromium carbides in the microstructure. The co-existence of Co and of Ni in the alloy's chemical composition is often in commercial superalloys. Indeed, Co brings solid solution strengthening to nickel-based alloys and Ni stabilizes the Face Centered Cubic crystal structure of cobalt alloys. Otherwise, adding cobalt to nickel bases may also favor the stability of TaC carbides and adding nickel to cobalt bases may enhance the resistance against high temperature oxidation by favoring chromium diffusion. Inversely, for the same reasons, adding cobalt to nickel alloys to favor the formation of tantalum carbides at the expense of chromium carbides may unfortunately deteriorate the oxidation resistance of the nickel alloys. This is this deleterious effect of Co addition for the high temperature oxidation resistance of tantalum-containing nickel-chromium alloys which will be studied in this work, by characterizing the behavior in oxidation at a rather high temperature of successive Ni-25Cr-0.4C-6Ta alloys in which Ni will be more and more replaced by Co.

2 Experimental details

2.1 Synthesis of the alloys

Six {Ni and/or Co}-25Cr-0.4C-6Ta alloys (all contents in wt.%) were fabricated by classical foundry, using a CELES high frequency induction furnace. Their chosen chemical compositions are displayed in Table 1. Parts of pure elements (Ni, Co, Cr and Ta: Alfa Aesar, graphite, all with purities higher than 99.9% in weight) were melted together, in a copper crucible cooled by a continuous flow of water. Heating of the mix, melting, {3 minutes}-stage in the molten state and cooling were carried out in inert gaseous condition (300 millibars of pure argon, chamber isolated from laboratory air by a silica tube). The applied operating parameters were 50kW (power) and about 100kHz (frequency).

2.2 The oxidation tests

The obtained ingots were similar to cones with a height of 22±1 mm, a basis diameter of 22±1 mm too, and a round top (radius of about 5mm). Their masses were of 40±1 grams for all. Each was cut in four parts of same mass and shape. A first part was kept for preparing the sample devoted to the control of the as-cast microstructures. A second part was especially prepared for the exposure at high temperature. The atmosphere to which they were exposed was the air present in the laboratory: close to 80%N_2 and 20%O_2 with presence of water vapor (close to 70% of relative humidity at 25°C). Before oxidation test all the samples were ground all around with 1200-grit SiC papers. These parts were placed in a Nabertherm muffle furnace, then exposed during 24 hours at a temperature wished higher than 1200°C. The heating rate was +15°C/min and the cooling rate was -5°C/min at the beginning and close to -1°C/min for the last part. The obtained temperature, which really remained constant +/- 2°C, was 1237°C.

2.3 Metallographic preparation

After high temperature exposure, the oxidized samples were covered by an extra-thin gold coating to allow their external surface to be electrically conductive despite the presence of the external oxides. Immersed in a 50°C-heated Watt's bath the gold-coated samples were polarized as cathodes. The constant 1.6 A/cm² current, applied during two hours between them and the nickel anodes, allowed obtaining a metallic nickel shell all around them, thick enough to protect the external scales during subsequent cutting. A metallographic Buehler Delta Abrasimet 5000 cutter allowed separating each sample in two parts for cross sections preparation. The samples were embedded in a cold resin mixture (ESCIL). The ones devoted to the observation of the as-cast microstructures and the ones for the cross-sectional characterization of the oxidation results were polished using SiC papers from 240-grit to 1200-grit. Water washing and ultrasonically cleaning were done to remove all possible attached SiC particles. Finally, the metallographic samples were polished with textile disks enriched by 1µm hard particles, until obtaining a mirror-like state.

2.4 Metallographic observations

The samples of the two types (as-cast microstructure and oxidation states) were examined by electron microscopy. The used scanning electron microscope (SEM) was a JEOL JSM-6010LA equipped with an Energy Dispersion Spectrometry (EDS) device. Imaging was done in the Back Scattered Electrons (BSE) mode, under 20kV. EDS full frame analysis was performed at the ×250 magnification for the control of the general chemical compositions of the alloys. For that three locations were randomly chosen. Spot analyses were also carried out to identify the present phases (microstructure of the alloy) and the different oxide types seen in the external scales or in the subsurface.

2.4 Thermodynamic calculations

Some stable equilibria states were computed to better anticipate or understand the microstructures of the alloys, and to anticipate some moderate changes in compositions. This was done using the Thermo-Calc software (version N) [17] and a database resulting of the enrichment of the SSOL one [18] with additional systems

involving Ta compulsory for valuable results. This enriched version of the database contained notably the descriptions of the Ta-Ni, Ta-Co, Ta-Cr, Co-Ta-C, Ni-Ta-C and Cr-Ta-C systems.

3 Results

3.1 Nominal chemical compositions and the corresponding theoretic stable states

The alloys are expected to contain 25wt.%Cr, 0.4wt.%C and 6wt.%Ta. The 25wt.%Cr should allow the alloys to to be chromia-forming thanks to this chromium content high enough. The 0.4wt.%C and 6wt.%Ta, weight contents corresponding to equal molar contents, would allow the formation of TaC exclusively. The rest is composed of 68.6 wt.% shared between Ni and Co. The system of designation of the alloys is the following one: the "Nix/5Co" alloy is the alloy containing $x/5 \times 68.6$ wt.% of cobalt and $(1-x)/5 \times 68.6$ wt.% of nickel. The resulting targeted compositions are displayed in Table 1. This is for these theoretic chemical compositions that the isopleth section of the Co-Ni-Cr-C-Ta phase diagram was computed and the six different alloys were positioned as vertical broken lines (Figure 1). It was considered that no significant diffusion-dependent solid state phase transformation can take place during cooling below 1000°C. Consequently the two nickel-richest alloys ("Ni0/5Co" and "Ni1/5Co") ought to contain chromium carbides (principally of the Cr_7C_3 type), and the two cobalt-richest alloys ("Ni4/5Co" and "Ni5/5Co") ought to contain only TaC as carbides. The two intermediate alloys ("Ni2/5Co" and "Ni3/5Co") may contain both kinds of carbides.

3.2 Actual chemical compositions and as-cast microstructures

By consulting Table 2 it appears that the wished compositions were globally well respected. The microstructures presented by the alloys in their as-cast state are illustrated by micrographs: in Figure 2 for the three Ni-richest alloys and in Figure 3 for the three Co-richest ones. In each case, general views of the microstructures are given in the top position (Fig. 2a-c and Fig. 3a-c). The microstructures are detailed and the carbides identified (spot EDS analysis) in the bottom position (Fig. 2a'-c' and Fig. 3a'-c'). The Ni0/5Co (Fig. 2a and a') and Ni1/5Co (Fig. 2b and b') alloys do contain Cr_7C_3 carbides but also TaC carbides, in significant quantities (more for Ni1/5Co than for Ni0/5Co). As expected, the two following alloys, Ni2/5Co (Fig. 2c and c') and Ni3/5Co (Fig. 3a and a') contain Cr_7C_3 (lower fractions by comparison with the formers) and TaC (higher fractions). The fraction of TaC was further increased in the Ni4/5Co (Fig. 3b and b') and Ni5/5Co (Fig. 3c and c') alloys, with only traces of chromium carbides here and there.

3.3 Oxidation behavior

The general deterioration (top micrographs) of the alloys after 24 hours at 1237°C in air are illustrated in Figure 4 for the two nickel-richest alloys (Ni0/5Co in Fig. 4a and Ni1/5Co in Fig. 4b), in Figure 5 for the intermediate alloys (Ni2/5Co in Fig. 5a and Ni3/5Co in Fig. 5b) and in Figure 6 for the two cobalt-richest alloys (Ni4/5Co in Fig. 6a and Ni5/5Co in Fig. 6b). The oxidation products are more detailed in the bottom micrographs of the same figures: Fig. 4a' and b', Fig. 5a' and b' and Fig. 6a' and b' respectively. In all cases oxidation seemingly led to both external and internal oxidation. The external scales have partly spalled off but parts remaining in quantities high enough allowed characterizing their compositions. These oxide scales are made of only chromia for the two nickel-richest alloys and the two intermediate ones. On the two cobalt-richest alloys a complex oxide involving both chromium and cobalt, the spinel $CoCr_2O_4$, also formed, together with chromia. The alloy/scale

interface is globally regular for the four first alloys and significantly irregular for the two last ones. This suggests that the oxidation process concerning the major constituents (Cr, Co, Ni) was essentially cationic in the first cases and more complex for the other cases. Another main oxidation product is the $CrTaO_4$ oxide. It is usually found for Ta-rich alloys [19, 20]. This oxide formed an almost continuous intermediate oxide, both internal and external just under chromia or under the chromia + spinel scale. Its formation obviously induced the appearance and the deepening of a carbide-free zone, in which tantalum carbides (and also chromium carbides) disappeared. Induced by the diffusion of Ta (and Cr) atoms towards the oxidation front, thermochemical unbalance appeared between the carbide phases and the matrix. This promoted the decomposition of the carbides to balance the local microstructure. Such phenomena were reported and interpreted in previous works. In a first one this is the general example of two-phase structures including a phase involving an element particularly reactive to oxidation which was explained [21]. This phenomenon was also reported for other examples. In the case of a Fe-15Cr-0.5C hot-forged alloy chromium carbides disappeared in the subsurface from the oxidation front [22]. For alloys composed of a Cr-based solid solution imbricated with a chromium silicide phase this is the disappearance of Cr_3Si in a zone progressively developed from the oxidation front which was noticed and commented [23]. These previous observations are very similar to what happened here for the chromium carbides too, and for tantalum carbides. Here again this is the most reactive elements, Cr an Ta, which oxidized preferentially on surface. This resulted in the impoverishment of the matrix in these two elements, which induced the destabilization of the Cr-rich particles and of the Ta-rich ones. These particles dissolved and the released Cr and Ta atoms were incorporated in solid solution in the matrix, before themselves diffusing towards the oxidation front.

3.4 Quantitative analysis of the surface and subsurface deteriorations

The thicknesses of the oxides scales externally formed were measured first, when possible. This was effectively not always possible because of the severe spallation which occurred for some alloys. Too rare parts of external oxides were kept on the Ni0/5Co and Ni2/5Coalloy and this did not allow assessing the thickness. Among the three nickel-based alloys, only the Ni1/5Co cross-sectional metallographic sample allowed proposing an average thickness. In contrast, the external oxides remained more significantly around each of the three cobalt-richest samples and it was thus more possible to measure the scale thickness in their cases. The obtained values are displayed in Table 3. These results show that all scales are thinner than 25µm, but without clear dependence on the cobalt content.

The depths of alloy subsurface having lost their initial carbides were also measured. The results are given in Table 4. It appears that the average depth of the carbide-free zone tends to globally decrease when the cobalt content in alloy increases.

Local chemical data were also acquired in the subsurface by carrying out EDS spot analyses. First the contents in chromium (first column of results in Table 5) and in tantalum (first column of results in Table 6) in extreme surface were specified. The obtained minimal chromium content measured close to the alloy/oxide scale interface obviously decreases from the Ni0/5Co alloy to the Ni5/5Co one, from 20wt.% down to 11wt.%. The tantalum content at the same location seems to behave as the chromium one, but less regularly.

Concentration profiles were acquired across the carbide-free zones of the six alloys. Some of the obtained profiles are presented as examples in Figure 7 (for one of the nickel-richest alloys), Figure 8 (for one of the

intermediate alloys) and Figure 9 (for one of the cobalt-richest alloys). In each case, the top graph gives the profiles of the main elements (Ni, Co, Cr) and the bottom graph enlarged the concentration profiles of tantalum. For these two elements one can see a concentration gradient. The local chromium content and the local tantalum one both decrease almost linearly when one moves toward the alloy/scale interface. This shows the diffusion of Cr and of Ta in the direction of the oxidation front. The average values of the gradients are given in the second column of results in Table 5 for Cr and Table 6 for Ta. The Cr gradient increases progressively from 0.03 wt.%/µm for the Ni0/5Co alloy to 0.14wt.% for the Ni5/5Co one. The evolution seems to be inverse for tantalum, with a gradient decreasing from 0.035wt.% to 0.025 wt.%. By considering that the external scales are almost of the same thickness for all alloys for a same oxidation duration (Table 3), the increase in Cr gradient from Ni0/5Co to Ni5/5Co suggests a diffusion of Cr less and less easy through the carbide-free zone. In contrast one cannot really conclude about tantalum. It is true that the Ta gradient becomes lower and lower from Ni0/5Co to Ni5/5Co, this evocating a Ta diffusion possibly helped by the presence of Co. But the values of gradients remain too close to one another to consider that they are really different, taking into account the limited accuracy of the EDS analysis.

4 Discussion

These six {Ni and/or Co}-based Cr-rich {Ta and C}-containing alloys, which were thus isothermally exposed at a very high temperature – 1237°C – for 24 hours, suffered high temperature oxidation and were subject to several well-known phenomena. These ones were: the formation of an external oxide scale, internal oxidation, the dissolution of the initially present carbides from the alloy/scale interface toward the bulk, and the diffusion of Cr and of Ta either initially present in solid solution in matrix or coming from the dissolving carbides. In all cases, at the end of the experiments, the major part of the Cr atoms having left the alloy is now present as Cr_2O_3 oxide while minor part has left the sample as gaseous CrO_3. Indeed the test temperature, much higher than 1000°C, is favorable to chromia re-oxidation in this volatile specie, but for so short oxidation duration the chromia scale thickening is predominant on the chromia loss by volatilization. Consequently to the presence of tantalum in significant quantity, a second type of oxide has appeared in the outer part of the alloy subsurface: $CrTaO_4$. A last common point for all the six alloys after high temperature test is the development of a carbide-free zone from the oxide scale/alloy interface, more or less extended toward the bulk, this depending on the Co/(Ni+Co) ratio of the alloy.

Both the bulk microstructural behavior and the high temperature oxidation behavior depend clearly on this Co/(Ni+Co) ratio. First it appeared here that replacing a part of nickel by cobalt in {25Cr-0.4C-6Ta, wt.%}-containing nickel-based alloys favor s the presence of TaC carbides instead chromium carbides. But this also obviously tends deteriorating the behavior of the alloys in oxidation at elevated temperature. The choice of a rather short high temperature oxidation duration − 24 hours only − was judicious since it showed here the start of catastrophic oxidation for the worst of the studied alloys, the cobalt-richest ones. These ones benefit from the presence of rather high contents in cobalt for obtaining an interdendritic network of mainly eutectic TaC with script morphology known as being very interesting for the mechanical resistance at elevated temperature. But they unfortunately also suffer from this Co presence in the field of oxidation.

This was not really surprising since one knows from several decades that cobalt-chromium alloys are generally less resistant against high temperature oxidation than nickel-chromium alloys. This was furthermore demonstrated here that this is also true in the case of alloys containing significant TaC carbides and/or high content in tantalum. In presence of 6wt.%Ta the alloys sufficiently rich in nickel and poor in cobalt may contain significant fraction of TaC and remain chromia-forming and oxidation resistant. The 6wt.%Ta-containing alloys rich in cobalt / poor in nickel benefit from the presence of more TaC carbides and from the absence of chromium carbides. Indeed the morphology of the TaC is much more stable at high temperature than the ones of the chromium carbides. Unfortunately, even after only 24 hours of oxidation at 1237°C, these alloys are progressively losing their chromia-forming behavior, as proven by the appearance of $CoCr_2O_4$ spinel oxides and even of CoO oxides. Here and there, the oxidation behavior seems starting to become catastrophic with the beginning of the inward progression of oxidation and the alloy consumption. The origin of this difference in oxidation behavior of these Ta-rich alloys rich in Ni or rich in Co appears to be the same as in other types of nickel-chromium and cobalt-chromium alloys: the increasing difficulty of Cr diffusion enhanced by the presence of more and more cobalt instead nickel. This was revealed by the possible Cr diffusion for the nickel-rich alloys from deeper zones than in the case of the cobalt-based ones. This resulted in both a more inward extended carbide-free zone but a higher Cr content in extreme surface for the nickel-rich alloys than for the cobalt-rich one.

The presence of 6wt.%Ta and of the associated high fraction of TaC carbides obviously does not change this effect. In contrast, the presence of 6wt.%Ta in all these alloys induced the development of another type of complex oxide, $CrTaO_4$, in great quantity. This oxide grows in the outer part of alloy, just under the external oxide scale, thanks to the progressive disappearance of the primary TaC carbides over a depth increasing with time, and the outward diffusion of the released Ta atoms. The role of these $CrTaO_4$ oxides on the general high temperature oxidation of the alloys remains to be specified. On the first hand one can imagine that, by constituting a rather dense second oxide barrier below the external chromia scale, its presence may be a little protective (but surely not as efficient as chromia) by separating a second time hot gases and alloy. This sub-layer, which may become totally continuous, may act as a second obstacle for the outward Cr diffusion. This may be detrimental for the behavior. In addition one can question about the impact of this $CrTaO_4$ sub-layer on the adherence of the external chromia scale during thermal cycling. Its presence surely changes totally the conditions of interaction between the alloy and the chromia scale. To answer this question one can envisage deeper investigations involving the double effect of both Ta contents and cooling rate on the scale spallation, by varying the Ta contents in alloy and the constant cooling rates.

After all these considerations one can focus again on the most vulnerable alloys in the high temperature oxidation field, the cobalt-richest ones. These alloys seem to be the most armed to resist mechanical stresses at high temperature thanks to their dense and rather morphologically stable carbides network (only TaC). But they are obviously too early threatened by catastrophic oxidation. To solve this problem one can envisage enriching them in chromium to enhance their resistance against oxidation by gases (and also corrosion by molten salts or glasses, for example) but this may induce negative consequences about the nature of their carbides. Indeed, by increasing the Cr content it is possible to favor the chromium car bides formation instead a part of the tantalum

ones. In order to anticipate such problem thermodynamic calculations may be of great help. In the present case an isopleth section of the Ni-Co-Cr-C-Ta diagram was calculated for the [0; 68.6wt.%] Co content range and the [1000; 1500°C] temperature range, the contents in Cr, C and Ta staying fixed at 25wt.%, 0.4wt.% and 6wt.% respectively (Figure 10). A second one for 30wt.%Cr instead 25wt.% was also calculated (Figure 11). By comparing the two diagrams, one can see that adding 5wt.%Cr more did not induce a significant movement of the high temperature {FCC matrix + Cr_7C_3 / FCC mat. + Cr_7C_3 + TaC} and {FCC matrix + Cr_7C_3 + TaC / FCC mat. + TaC} frontiers towards the left of the diagram as this can be expected by considering that more Cr may promote chromium carbides to the detriment of TaC. Instead, the noticeable obtained frontier movement is the 200°C-increase of the temperature of the Cr_7C_3 – $Cr_{23}C_6$ transition. In case of isothermal work under applied stresses at high temperature, 1100°C for example, the microstructures of some of the cobalt-richest alloys may thus include $Cr_{23}C_6$ carbides beside TaC. The consequences of the presence of these chromium carbides belonging to a new type on the high temperature mechanical resistance remain to be investigated.

Concerning the double-phased state matrix + TaC of the cobalt-richest alloys, the displacement to higher temperatures of the {FCC matrix + TaC + $Cr_{23}C_6$ / FCC mat. + TaC} frontier induces a significant decrease in the temperature range for the Co4/5Ni alloy, because of the lower slope of dependence on the Co content by comparison with the same frontier but involving Cr_7C_3. Indeed, only double-phased {FCC matrix + TaC} from 1050°C up to the melting start temperature when containing 25wt.%Cr, this alloy is double-phased {FCC matrix + TaC} only for temperatures higher than about 1125°C. In these conditions, one must consider that a part of carbon is present, not in the morphologically stable TaC as the other part, but as chromium carbides which rapidly evaluate to a round shape and then become useless for the mechanical resistance. Such effect may be without any detrimental consequence for the global mechanical behavior of the alloy at high temperature if limited to a thin outer part, as achievable by pack-cementation Cr deposition, for example.

5 Conclusion

Adding cobalt to nickel-based 25wt.%Cr-containing alloys in which C and Ta are also present in equivalent molar proportion succeeds in stabilizing the TaC phase. Moderate additions allow obtaining stable microstructures containing mainlyTaC coexisting with few chromium carbides while additions beyond a critical Co content lead to TaC exclusively. Unfortunately this work also reveals that the high temperature oxidation behavior of the obtained alloys, rich enough in Co to contain TaC as single carbide have become significantly worse than the initial alloy. One can guess that this behavior deterioration occurs for a higher critical Co content for shorter durations or for lower temperatures and inversely for a lower critical Co content for longer durations or for higher temperatures. Further work is needed to investigate the dependence of the critical Co content (which can be considered to be about 30wt.% in the present case: 1237°C, 24h) on the (temperature, duration) couple.

Rating the Co content to values leading to a carbide network made of TaC exclusively to benefit from their high mechanical strengthening effect at high temperature is unfortunately detrimental for the oxidation resistance to hot air. It is possible to benefit from both high temperature strength and high oxidation resistance by decoupling the properties required for the bulk and for the surface, this by choosing a Co content high enough for the bulk to stabilize the TaC carbides and by enriching the outer part of the alloy in chromium. Recent work precisely

demonstrated that this is precisely possible for TaC-containing Cr_xC_y-free Cr rich {cobalt, nickel}-based alloys [24] with significant improvement of the high temperature oxidation behavior when the Cr content obtained in subsurface is 30wt.% [25]. The thermodynamic calculations carried out in the present work showed that such resulting enrichment did not induce any serious problem for the microstructure of the Cr-enriched outer zone.

References:

[1] P. T. B. Shaffer, *Handbook of High-Temperature Materials: N°1 Materials Index*, Plenum Press, New York **1964**.

[2] G. V. Samsonov, *Handbook of High-Temperature Materials: N°2 Properties Index*, Plenum Press, New York **1964**.

[3] M. Durand-Charre, *The Microstructure of Superalloys*, CRC Press, Boca Raton **1997**.

[4] C. T. Sims, W. C. Hagel, *The Superalloys*, John Wiley and Sons, New York **1972**.

[5] E. F. Bradley, *Superalloys: A technical guide*, ASM International, Metals Park **1988**.

[6] H. Morrow, W. P. Danesi, D. L. Sponseller, Cobalt **1973**, *4*, 93.

[7] R. L. Ammon, L. R. Eisenstatt, G. O. Yatsko, Journal of Engineering for Power **1981**, *103(2)*, 331.

[8] J. Reuchet, L. Remy, Metallurgical Transactions A: Physical Metallurgy and Materials Science **1983**, *14(1)*, 141.

[9] P. Berthod, Advances in Materials Science and Engineering **2017**, article ID 4145369, https://doi.org/10.1155/2017/4145369.

[10] P. Berthod, Advanced Materials Letters **2017**, *8(8)*, 866.

[11] M. J. Donachie, S. J. Donachie, *Superalloys: A Technical Guide (2nd Edition)*, ASM International, Materials Park **2002**.

[12] P. Kofstad, *High temperature corrosion*, Elsevier applied science, London **1988**.

[13] D. Young, *High Temperature Oxidation and Corrosion of Metals*, Elsevier Corrosion Series, Amsterdam **2008**.

[14] P. Berthod, S. Michon, L. Aranda, S. Mathieu, J. C. Gachon, Calphad **2003**, *27*, 353.

[15] P. Berthod, Y. Hamini, L. Aranda, L. Héricher, Calphad **2007**, *31*, 351.

[16] P. Berthod, L. Aranda, C. Vébert, S. Michon, Calphad **2004**, *28*, 159.

[17] Thermo-Calc version N: "Foundation for Computational Thermodynamics" Stockholm, Sweden, Copyright (1993, 2000). www.thermocalc.com

[18] SSOL database, SGTE Solutions Database, Scientific Group Thermodata Europe, Bo Sundman, Stockholm, Sweden.

[19] P. Berthod, S. Raude, A. Chiaravalle, Annales de Chimie – Science des Matériaux, **2006**, *31(2)*, 237.

[20] P. Berthod, L. Aranda, C. Vébert, Annales de Chimie – Science des Matériaux **2006**, *31(2)*, 213.

[21] F. Gesmundo, B. Gleeson, Oxidation of Metals **1995**, *44(1/2)*, 211.

[22] M. P. Brady, B. Gleeson, I. G. Wright, JOM **2000**, *52(1)*, 16.

[23] A. Soleimani Dorcheh, M. C. Galetz, Oxidation of Metals **2016**, DOI: 10.1007/s11085-016-9685-1, in press.

[24] G. Michel, P. Berthod, M. Vilasi, S. Mathieu, P. Steinmetz, Surface & Coatings Technology **2011**, *205*, 3708.

[25] G. Michel, P. Berthod, M. Vilasi, S. Mathieu, P. Steinmetz, Surface & Coatings Technology **2011**, *205*, 5241.

TABLES

Table 1. Compositions wished for the six alloys of the study (in wt.%).

Alloys	Ni	Co	Cr	Ta	C
“Ni0/5Co”	Bal.	0	25	6	0.4
“Ni1/5Co”	Bal.	13.7	25	6	0.4
“Ni2/5Co”	Bal.	27.4	25	6	0.4
“Ni3/5Co”	27.4	Bal.	25	6	0.4
“Ni4/5Co”	13.7	Bal.	25	6	0.4
“Ni5/5Co”	0	Bal.	25	6	0.4

Table 2. Chemical compositions of the obtained alloys (weight contents); average and standard deviation of three full-frame SEM/EDS measurements carried out at the ×250 magnification)

Alloys	Ni	Co	Cr	Ta	C
“Ni0/5Co”	Bal.	/	25.5 ±0.1	6.5 ±0.2	“0.4”*
“Ni1/5Co”	Bal.	14.3 ±0.2	25.4 ±0.4	5.6 ±0.9	“0.4”*
“Ni2/5Co”	Bal.	27.2 ±0.2	25.4 ±0.1	6.5 ±0.2	“0.4”*
“Ni3/5Co”	25.4 ±0.3	Bal.	25.7 ±0.4	6.9 ±0.2	“0.4”*
“Ni4/5Co”	12.7 ±0.5	Bal.	26.2 ±0.2	6.6 ±0.8	“0.4”*
“Ni5/5Co”	/	Bal.	25.3 ±0.2	7.2 ±0.5	“0.4”*

*: C not controlled by EDS; supposed to be correctly respected according to the experience acquired for long time for this elaboration procedure; confirmed by the obtained density of carbides

Table 3. Average and standard deviations (from 10 measurements) of the thickness of the external oxide scale (first results column) for the six alloys oxidized for 24 hours at 1237°C

Alloys	Oxide scale thickness (µm)
"Ni0/5Co"	Not available (too severe spallation)
"Ni1/5Co"	17.0 ±5.5
"Ni2/5Co"	Not available (too severe spallation)
"Ni3/5Co"	21.0 ±4.3
"Ni4/5Co"	11.9 ±4.6
"Ni5/5Co"	22.5 ±4.4

Table 4. Average and standard deviations of the carbide-free depth for the six alloys oxidized for 24 hours at 1237°C

Alloys	Carbide-free zone depth (µm)
"Ni0/5Co"	128 ±8
"Ni1/5Co"	98 ±8
"Ni2/5Co"	85 ±5
"Ni3/5Co"	88 ±10
"Ni4/5Co"	90 ±12
"Ni5/5Co"	84 ±7

Table 5. Average and standard deviation for the chromium content in extreme surface (three measurements) for the six alloys oxidized for 24 hours at 1237°C

Alloys	Chromium content in extreme surface (wt.%)	Cr-gradient (wt.% / µm)
"NiCo0"	19.8 ±0.3	0.028
"NiCo1"	19.6 ±0.1	0.041
"NiCo2"	17.7 ±0.5	0.049
"NiCo3"	17.5 ±0.2	0.046
"NiCo4"	11.0 ±0.4	0.112
"NiCo5"	10.6 ±1.0	0.136

Table 6. Average and standard deviation for the tantalum content in extreme surface (three measurements) for the six alloys oxidized for 24 hours at 1237°C

Alloys	Tantalum content in extreme surface (wt.%)	Ta-gradient (wt.% / µm)
"NiCo0"	1.8 ±0.3	0.035
"NiCo1"	1.9 ±1.2	0.033
"NiCo2"	0.7 ±0.1	0.030
"NiCo3"	0.8 ±0.3	Too perturbed profile for allowing gradient accurate enough
"NiCo4"	0.4 ±0.2	0.030
"NiCo5"	0.7 ±0.1	0.026

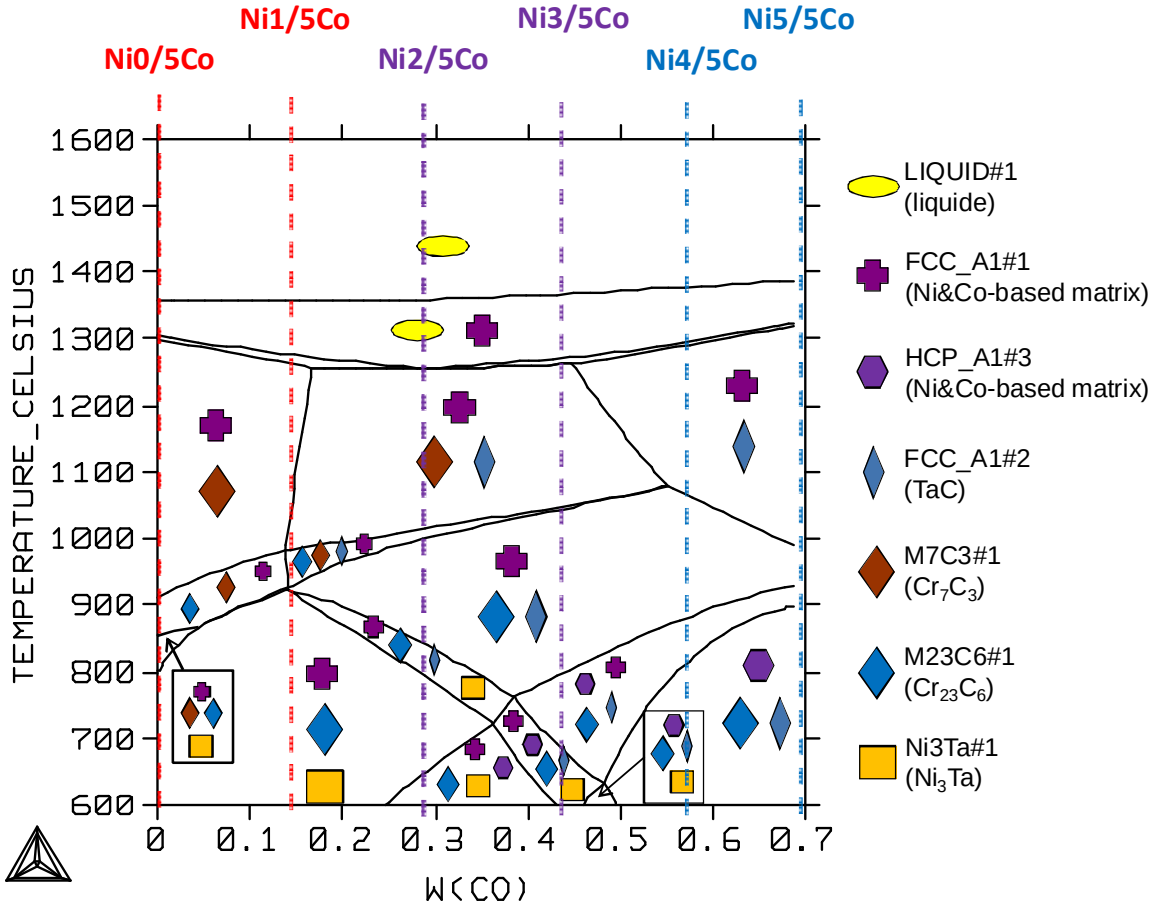

Figure 1. {25Cr, 0.4C, 6Ta}-isopleth section of the Co-Ni-Cr-C-Ta diagram (computed using Thermo-Calc)

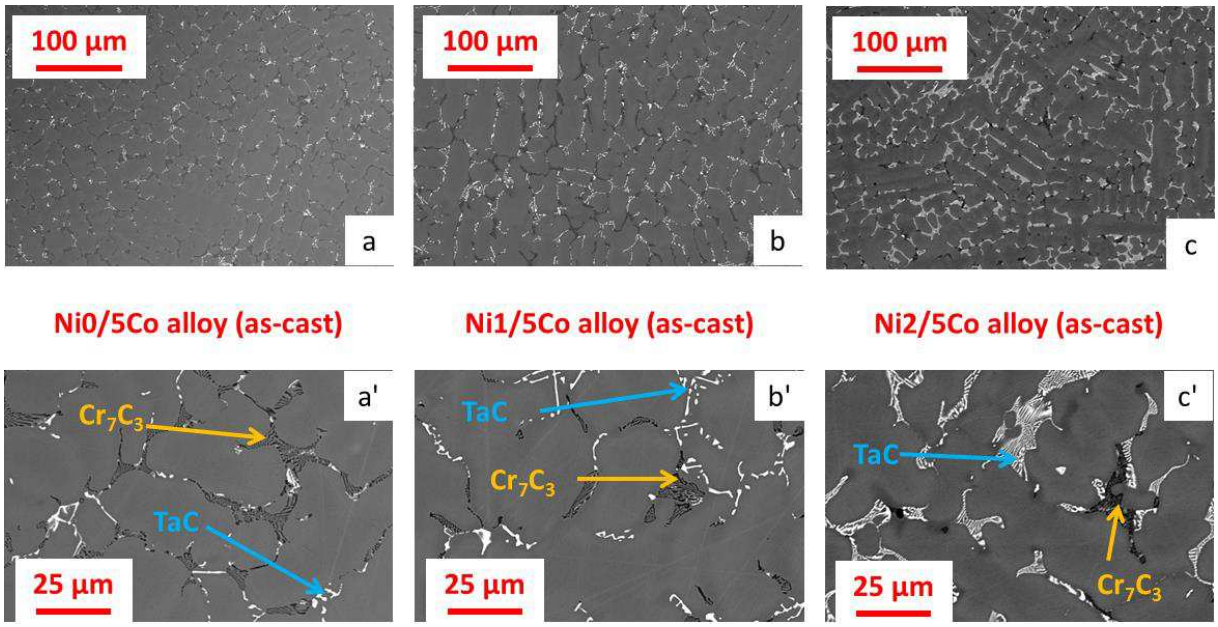

Figure 2. The as-cast microstructures of the three nickel-based alloys: Ni0/5Co alloy (a, a'), Ni1/5Co alloy (b, b') and Ni2/5Co alloy (c, c'); SEM/BSE micrographs taken at ×250 (a, b, c) or ×1000 (a', b', c')

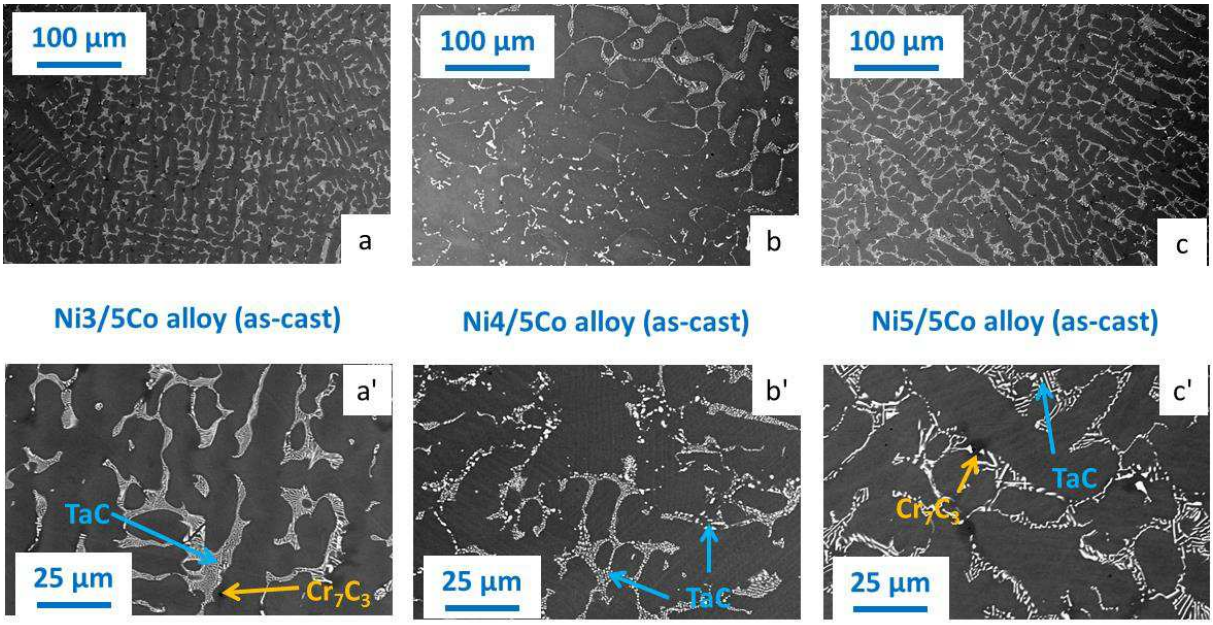

Figure 3. The as-cast microstructures of the three cobalt-based alloys: Ni3/5Co alloy (a, a'), Ni4/5Co alloy (b, b') and Ni5/5Co alloy (c, c'); SEM/BSE micrographs taken at ×250 (a, b, c) or ×1000 (a', b', c')

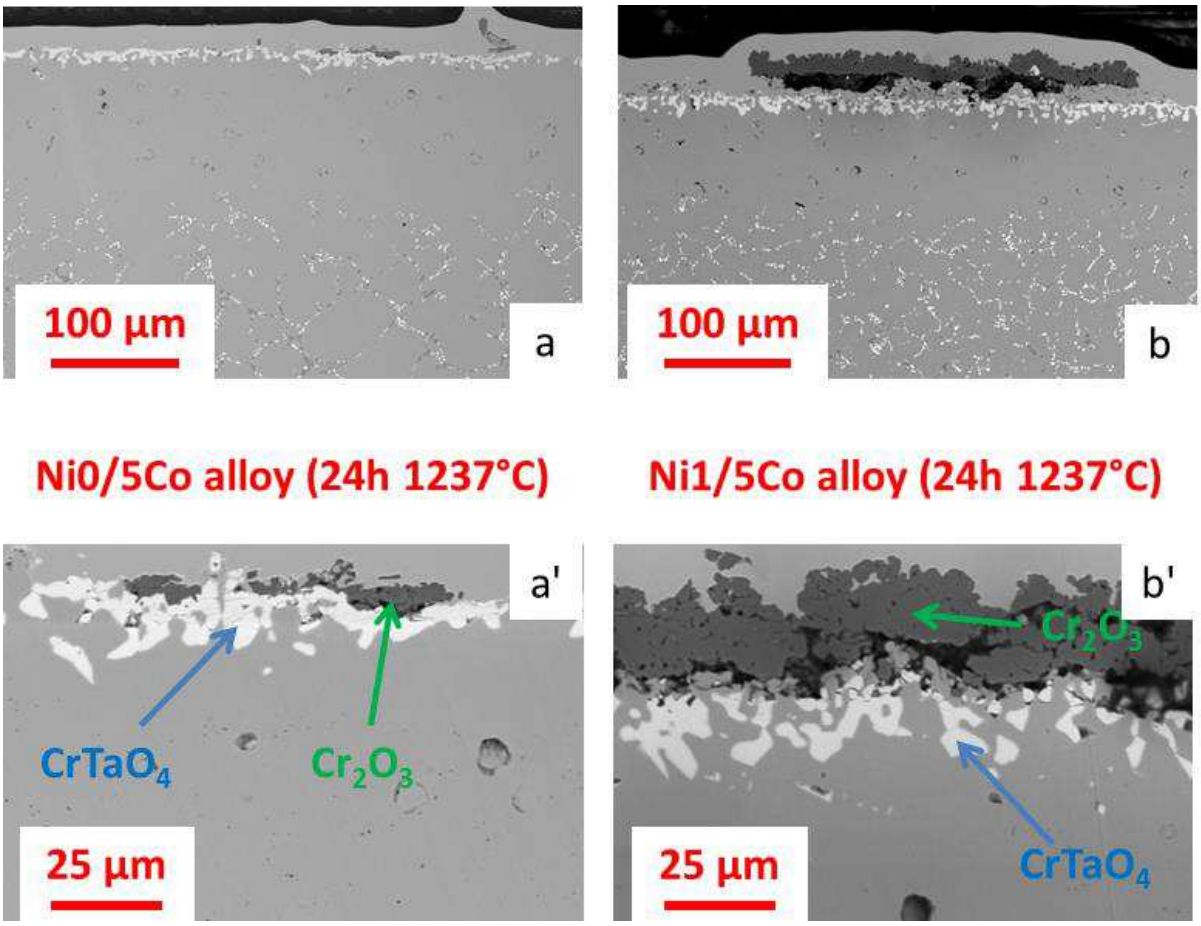

Figure 4. Enlarged views (top) of the surface oxidized states of the two nickel-richest alloys and corresponding detailed views (bottom) with identification of the corrosion products: Ni0/5Co alloy (a, a') and Ni1/5Co alloy (b, b'); SEM/BSE micrographs taken at ×250 (a, b) or ×1000 (a', b')

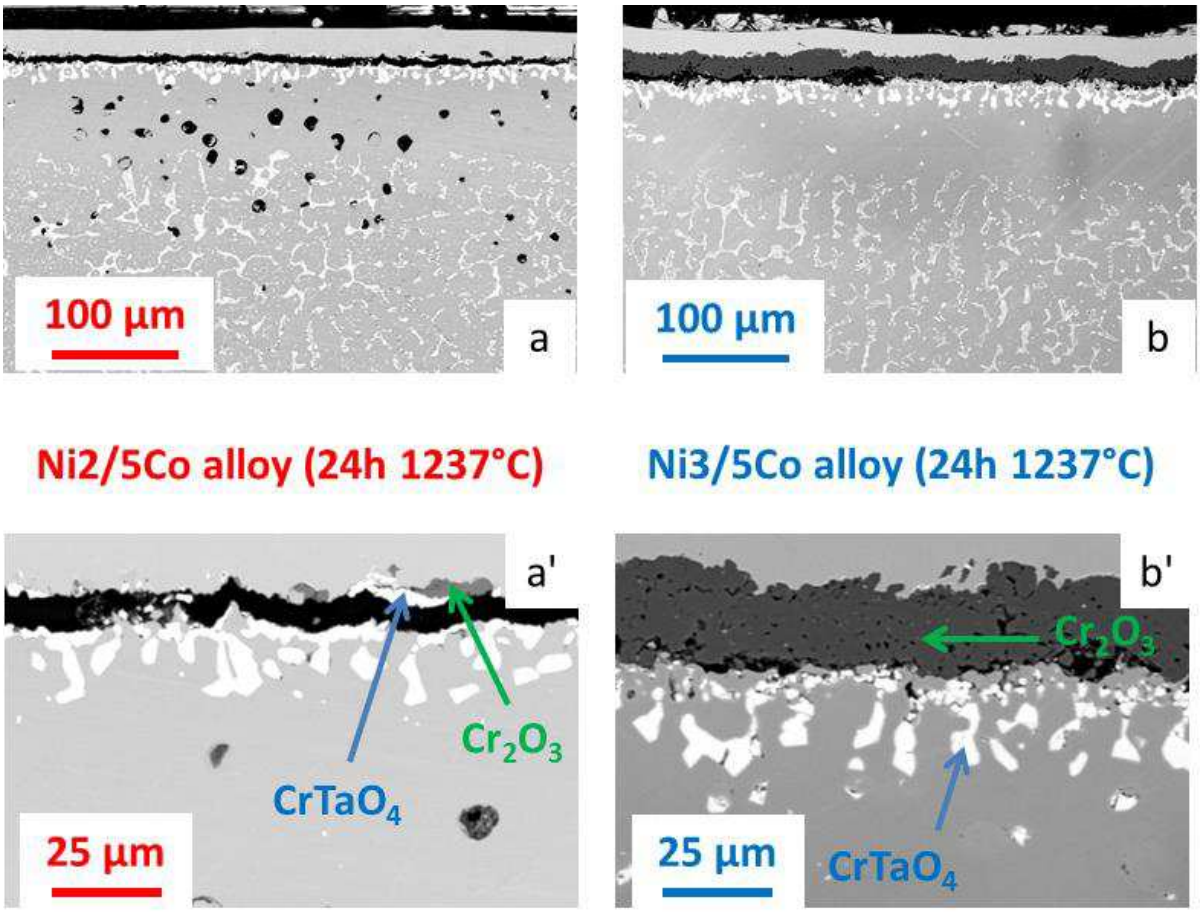

Figure 5. Enlarged views (top) of the surface oxidized states of the two medium alloys and corresponding detailed views (bottom) with identification of the corrosion products: Ni2/5Co alloy (a, a') and Ni3/5Co alloy (b, b'); SEM/BSE micrographs taken at ×250 (a, b) or ×1000 (a', b')

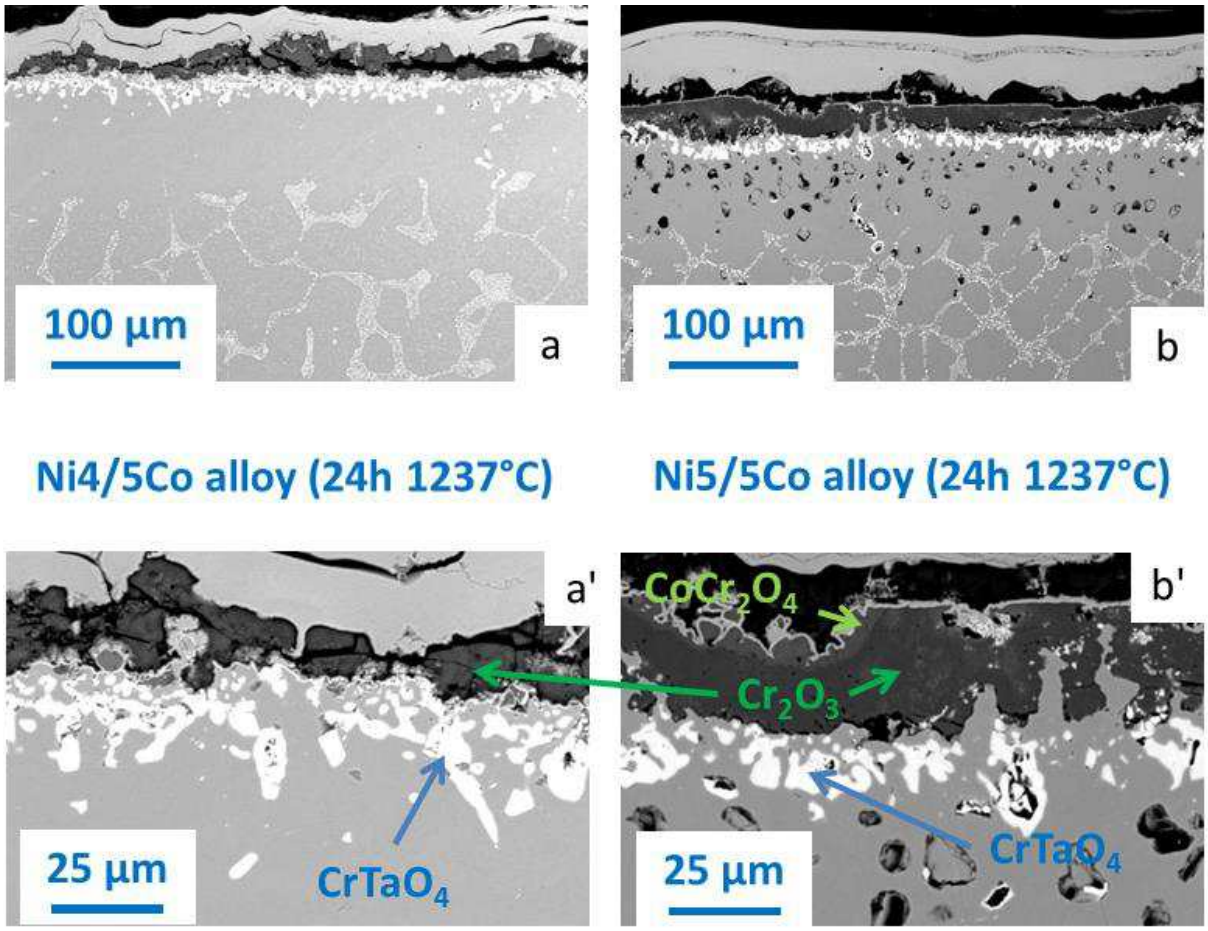

Figure 6. Enlarged views (top) of the surface oxidized states of the two cobalt-richest alloys and corresponding detailed views (bottom) with identification of the corrosion products: Ni4/5Co alloy (a, a') and Ni5/5Co alloy (b, b'); SEM/BSE micrographs taken at ×250 (a, b) or ×1000 (a', b')

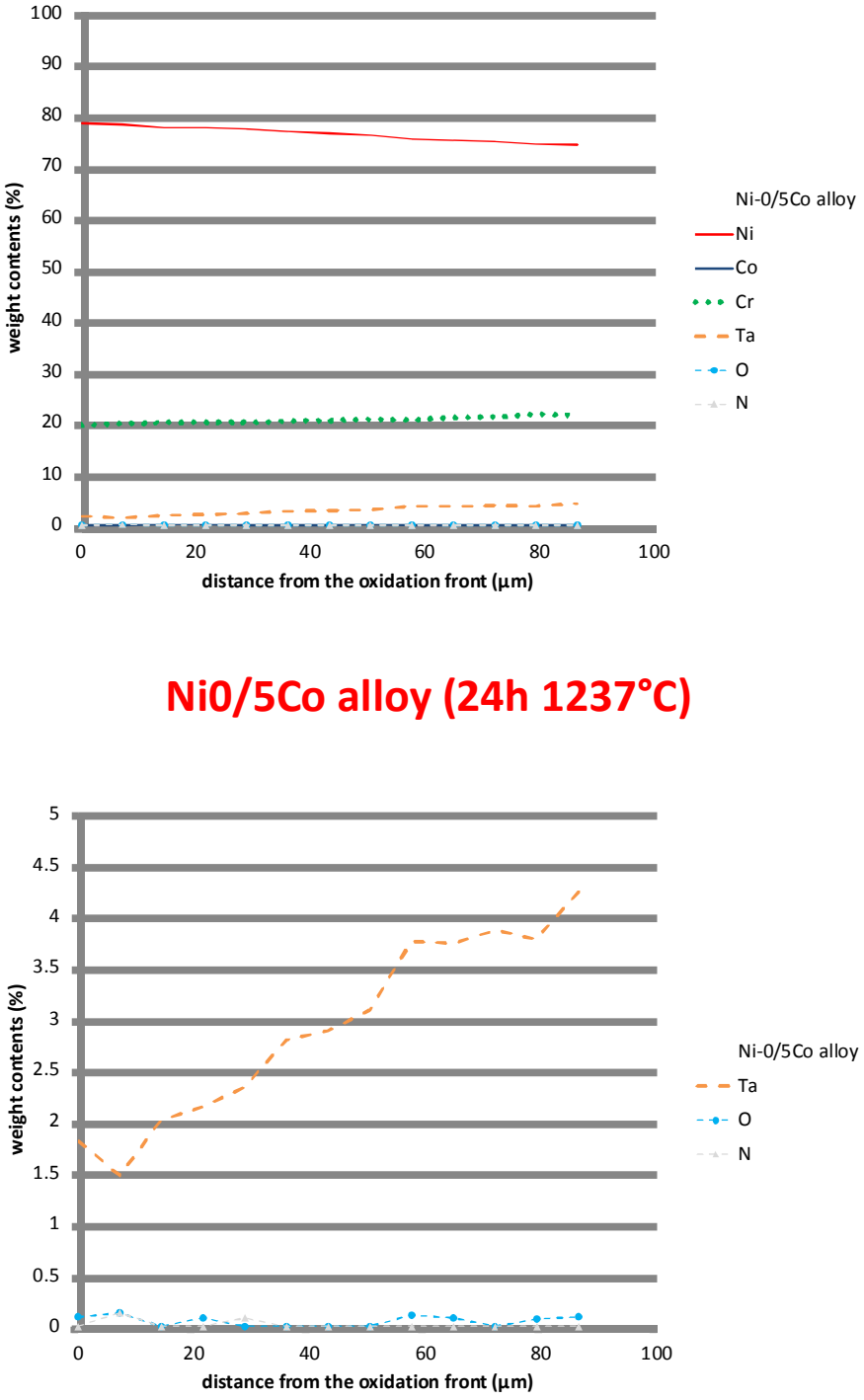

Figure 7. Example of concentration profiles acquired from and perpendicularly to the external oxide scale / alloy interface for one of the nickel-richest alloys after oxidation

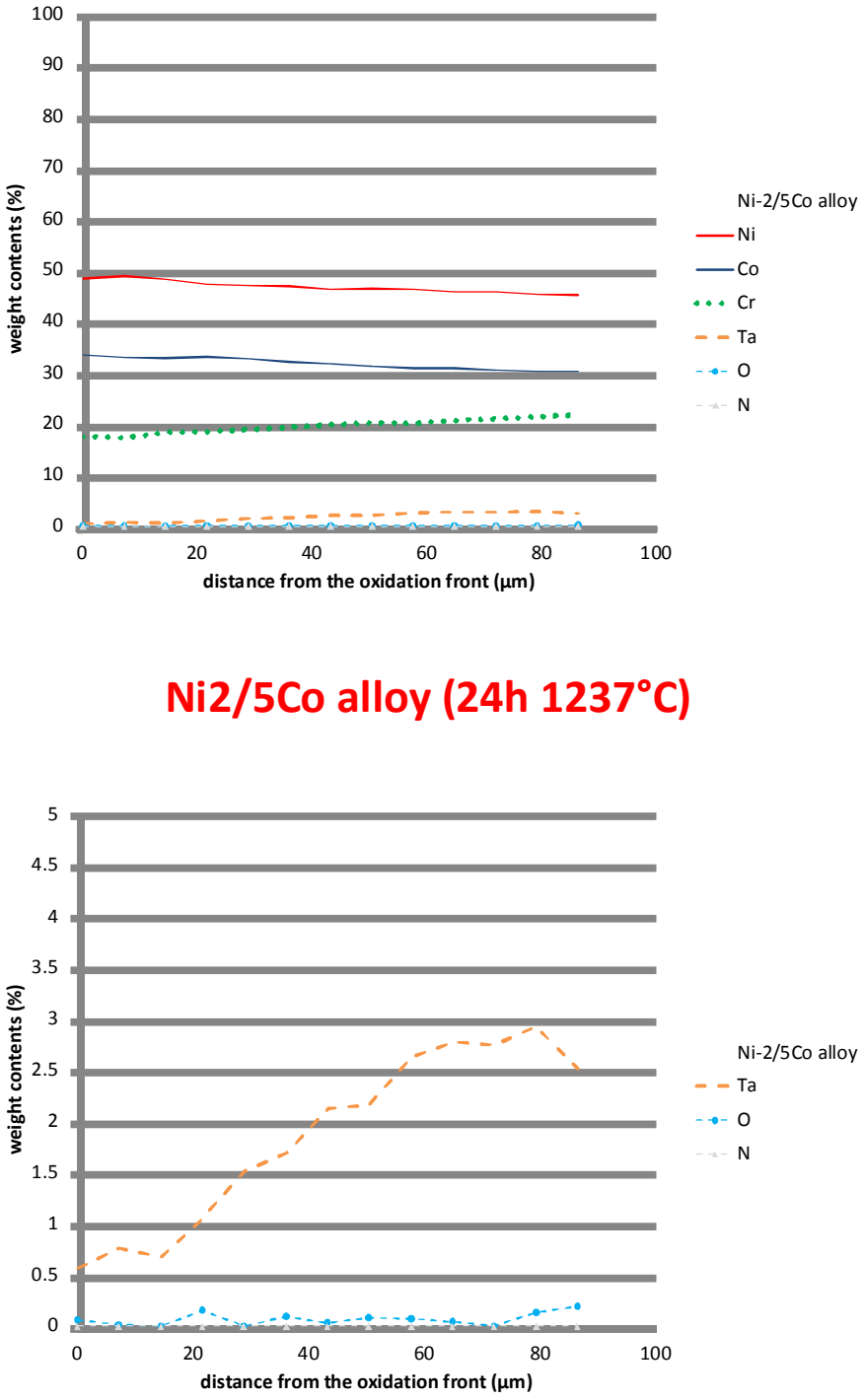

Figure 8. Example of concentration profiles acquired from and perpendicularly to the external oxide scale / alloy interface for one of the medium alloys after oxidation

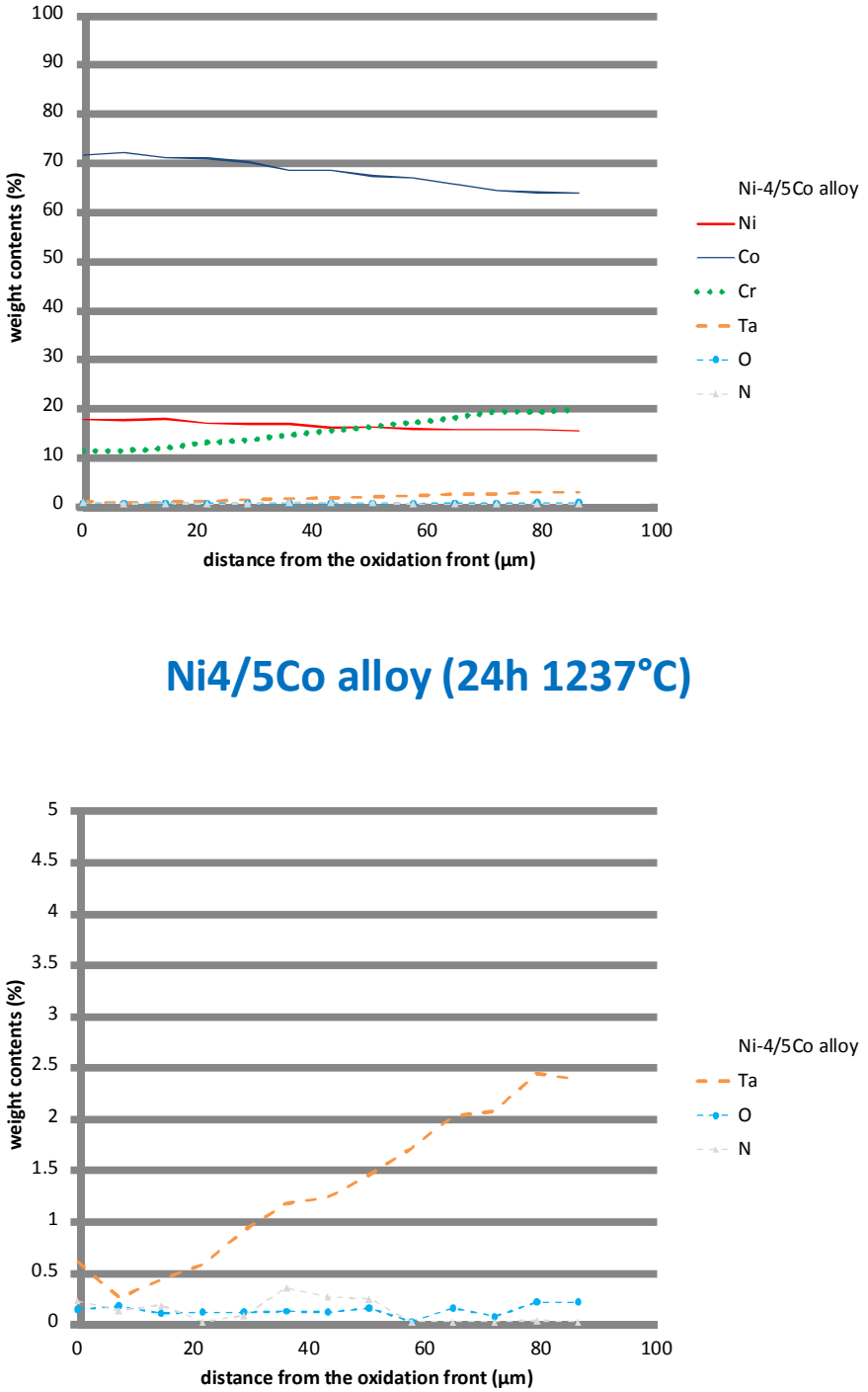

Figure 9. Example of concentration profiles acquired from and perpendicularly to the external oxide scale / alloy interface for one of the cobalt-richest alloys after oxidation

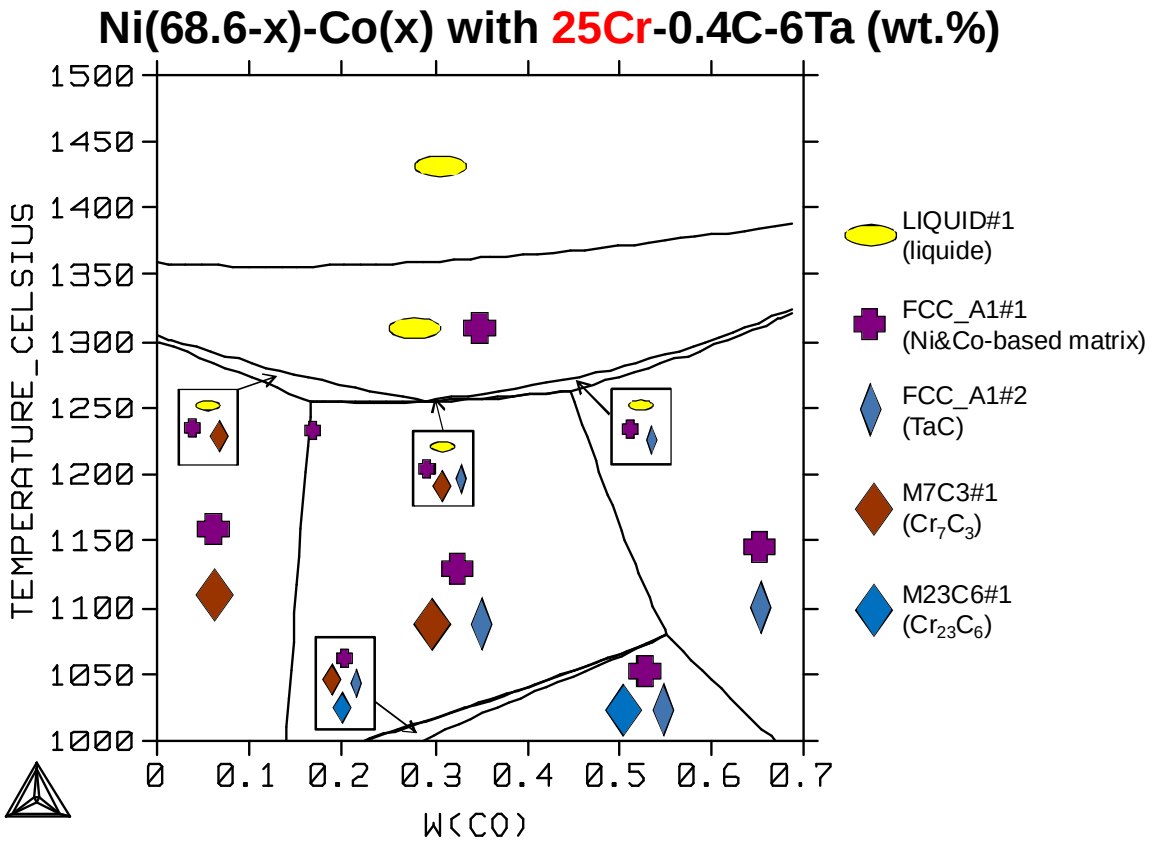

Figure 10. {1000-1500°C}-view of the {25Cr, 0.4C, 6Ta; wt.%}-section of the Ni-Co-Cr-C-Ta diagram

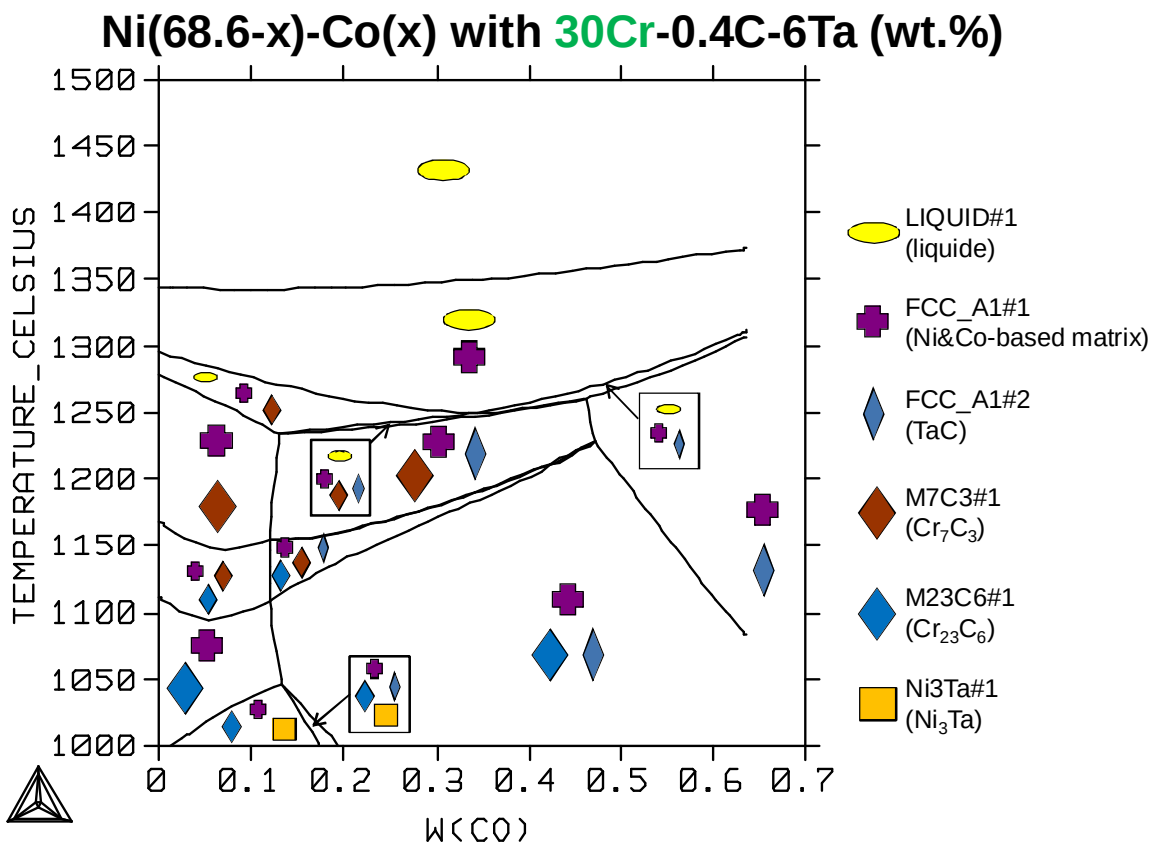

Figure 11. {1000-1500°C}-view of the {30Cr, 0.4C, 6Ta; wt.%}-section of the Ni-Co-Cr-C-Ta diagram; theoretic consequences of a 5wt.%Cr addition of the high temperature microstructures